Hindawi Publishing Corporation
Journal of Nanomaterials
Volume 2014, Article ID 298021, 10 pages
http://dx.doi.org/10.1155/2014/298021

Research Article

PAN Nanofibers Reinforced with MMT/GO Hybrid Nanofillers

Qingqing Wang,[1] Guohui Li,[1] Jinning Zhang,[1] Fenglin Huang,[1] Keyu Lu,[2] and Qufu Wei[1]

[1] *Key Laboratory of Eco-Textiles, Jiangnan University, Wuxi 214122, China*
[2] *State Key Laboratory of Food Science and Technology, Wuxi 214122, China*

Correspondence should be addressed to Qufu Wei; qfwei@jiangnan.edu.cn

Received 18 December 2013; Accepted 7 April 2014; Published 30 April 2014

Academic Editor: Sheng-Rui Jian

Single component nanofiller has shown some limitations in its performance, which can be overcome by hybrid nanofillers with two different components. In this work, montmorillonite (MMT)/graphene oxide (GO) hybrid nanofillers were formed by self-assembly and then incorporated into the polyacrylonitrile (PAN) nanofibers by electrospinning process. X-ray diffraction (XRD), atomic force microscopy (AFM), and transmission electron microscopy (TEM) were utilized to analyze the structures of MMT/GO hybrid nanofillers. And the effects of MMT/GO hybrid nanofillers on the morphology, thermal stability, and mechanical properties of PAN/MMT/GO composite nanofibrous membrane were examined by scanning electron microscopy (SEM), thermogravimetric analysis (TGA), and tensile test machine, respectively. The incorporation of MMT/GO hybrid nanofillers into PAN nanofibers showed a noticeable increase up to 30°C for the onset decomposition temperature and 1.32 times larger tensile strength than the pure PAN, indicating that the hybrid nanofiller is a promising candidate in improving thermal and mechanical properties of polymers.

1. Introduction

Among all the layer-structured materials, montmorillonite (MMT) and graphene oxide (GO) are most widely studied. MMT, a layered aluminosilicate mineral, consists of an octahedral gibbsite layer sandwiched between two tetrahedral silicate layers [1]. It has been well explored for its potential application as nanofillers for improving the mechanical and thermal properties of the guest polymers [2–4]. However, it was found that while MMT can increase the tensile strength and Young's modulus of the host polymer, the elongation at break was considerably decreased [5, 6].

Meanwhile, GO and nanoscale graphene platelet (NGP) are another emerging class of nanomaterials. In 2008, Jang and Zhamu [7] predicted that NGP's application as a nanofiller in a composite material was imminent. The prediction was based on detailed discussion of earlier processes, current developments, and some physical constants required by the nanofiller. The later publications proved his foresight. Since 2009, GO and NPG have been widely investigated as nanofillers for various polymers. It has been found that they can greatly enhance mechanical properties at very low content [8–10]. Due to the intrinsic hydrophilic property of GO, the polymers that can be reinforced by GO are very limited.

In view of this, self-assembly of the two different layered solids (MMT and GO) to form hybrid nanofillers in which the two different layers are interactional would be a promising way to solve this problem. The fabrication of MMT/GO or MMT/graphene composites has been reported [1, 11]. However, all the processes were accomplished in aqueous solution. As is known, most polymers can only be dissolved in organic solvents instead of water. So it is important to study the self-assembly behavior of MMT and GO in organic solvent system.

Recent works have shown some striking synergies in binary system of carbon nanotubes (CNTs)/GO hybrid nanofillers [12, 13]. As far as we are concerned, MMT/GO hybrid nanofillers used in polymer matrix have not been investigated yet. In this work, organically modified MMT was used as stabilizer for GO in DMF solvent. The MMT/GO hybrids prepared by self-assembly were investigated, and

their potential application as nanofiller was evaluated by being incorporated into electrospun PAN nanofibers.

2. Materials and Methods

2.1. Materials. The hexadecyl trimethyl ammonium bromide (CTAB) modified MMT was supplied by Zhejiang Fenghong Clay Chemicals Co., Ltd. (Zhejiang, China). The cation exchange capacity (CEC) of this MMT is 97 mequiv./100 g of clay. GO was purchased from XF Nano, Inc. (Nanjing, China). PAN (Mw = 50,000 $gmol^{-1}$) was obtained from Shangyu Wu & Yue Economic and Trade Co., Ltd. (Zhejiang, China). N,N-dimethylformamide (DMF) was purchased from Sinopharm Chemical Reagent Co., Ltd. (Shanghai, China). All chemicals were used without further purification.

2.2. Preparation and Characterization of the MMT/GO Hybrids. In this process, MMT and GO nanoparticles were separately dispersed in DMF before blending (Figure 1 inset). Four MMT/DMF suspensions were obtained by adding certain amount of MMT into 10 mL DMF. After repeated magnetic stirring and sonication for about 3 h, the uniform dispersions were obtained. As is seen in Figure 1 inset (a–d), from left to right, they represent 150 mg, 135 mg, 120 mg, and 105 mg MMT nanoparticles dispersed in 10 mL DMF, respectively. Meanwhile, three GO (15 mg, 30 mg, and 45 mg)/DMF (10 mL) suspensions (corresponding to Figure 1 insets b′, c′, and d′) were prepared in the same way. Then, the MMT and GO solutions were mixed together by magnetic stirring accompanied with sonication to obtain a total amount of solute at 150 mg with different weight ratios of MMT/GO as 10 : 0, 9 : 1, 8 : 2, and 7 : 3, as is shown in Figure 1 insets (a + 10 mL DMF, b + b′, c + c′, and d + d′). The as-prepared MMT/GO hybrid solutions were left there for further experiments.

The X-ray diffraction (XRD) experiments were employed here to investigate the "d space," which is the distance between the two adjacent layers of MMT, which is helpful in understanding the self-assembly behavior between MMT and GO in DMF. The MMT/GO hybrids in the solid form for XRD tests were obtained by vacuum filtration, repeated washing, vacuum drying at 65°C, and grinding. The experiments were carried out in a Philips MPD-18801 diffractometer using Cu Kα (λ = 0.15406 nm) radiation and a fixed power source (40 kV, 40 mA).

Atomic force microscopy (AFM) (Benyuan CSPM 4000) was used in this work to observe the surface morphology and phase homogeneity of the MMT/GO hybrids. The samples were prepared by applying one droplet of the MMT/GO hybrid solution to the surface of a freshly peeled mica and drying in oven under 40°C. All the AFM images were obtained in the tapping mode.

A Hitachi H-7500 transmission electron microscope (TEM) was used here to further examine the assembly behavior of the MMT/GO hybrids. The MMT/GO hybrids with the weight ratio of 8 : 2 were chosen for this study. One droplet of the hybrid solution was applied to the surface of the grid and dried under infrared lamp. The experiments were operated under the voltage of 80 kV.

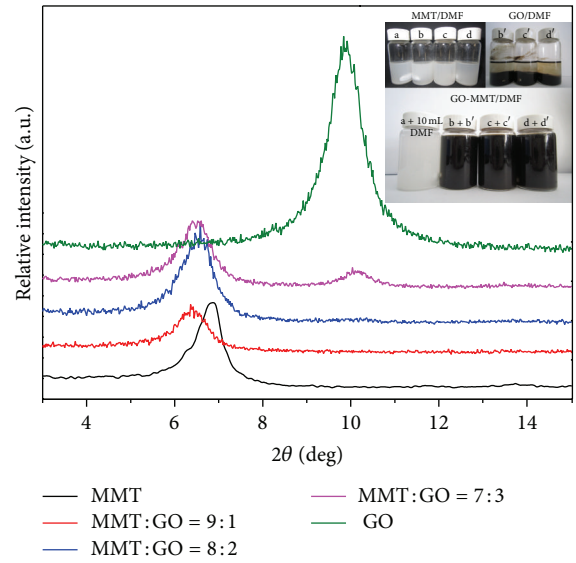

Figure 1: XRD patterns of MMT and GO and their hybrids assembled in DMF with different weight ratio; the inset shows the digital photographs of MMT (a–d, a: 150 mg, b: 135 mg, c: 120 mg, and d: 105 mg) and GO (b′–d′, b′: 15 mg, c′: 30 mg, and d′: 45 mg) dispersions in DMF (10 mL) and the blend of these two. The samples were left still for 24 h before capturing pictures.

2.3. Preparation and Characterization of PAN/MMT-GO Composite Electrospinning Solution and Electrospun Nanofibrous Membrane. The electrospinning solutions were prepared by adding 3 g PAN powders into the as-prepared MMT/GO hybrid DMF solution and magnetically stirring for about 24 h until homogeneous solution formed. The viscosity (NDJ-79), conductivity (DDS-11C), and surface tension (QBZY) of the electrospinning solutions were measured.

Then, the solutions were electrospun at a positive voltage of 15 kv with a working distance of 15 cm and a flow rate of 0.5 mL/h. The morphology of the electrospun nanofibers was characterized by scanning electron microscope (SEM) (Quanta 200, Holland FEI Company). The samples were sputter-coated with a thin layer of Au nanoparticles to reduce the charging effects. The SEM images were analyzed by Adobe Acrobat 7.0 Professional software to measure the fiber diameter, and 100 individual measurements were made on each sample to determine the mean diameter and standard deviation. The as-prepared electrospun composite nanofibers from solutions with different MMT/GO weight ratio were denoted as PAN/MMT-GO-1 (MMT : GO = 9 : 1), PAN/MMT-GO-2 (MMT : GO = 8 : 2), and PAN/MMT-GO-3 (MMT : GO = 7 : 3).

2.4. Thermal and Mechanical Properties of the PAN/MMT-GO Composite Nanofibers. Thermal properties were evaluated by the thermogravimetric analyses (TGA). They were carried out on a TGA-Q5000 thermoanalyzer instrument in

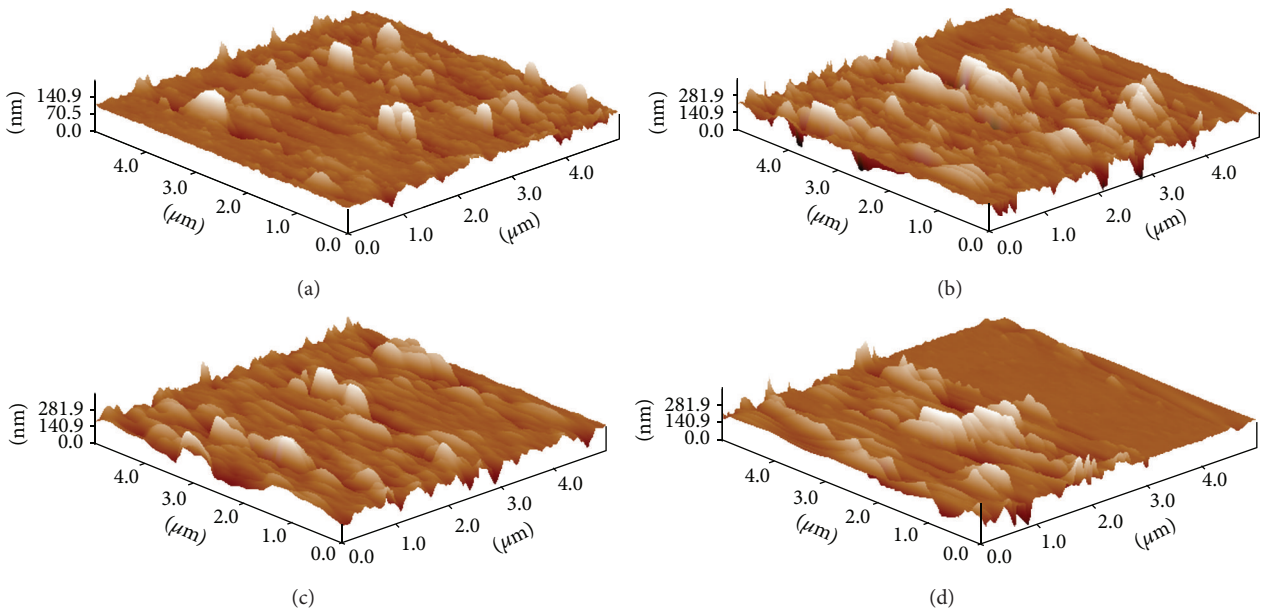

FIGURE 2: Tapping mode topography of the MMT and MMT/GO complexes: (a) MMT, (b) MMT : GO = 9 : 1, (c) MMT : GO = 8 : 2, and (d) MMT : GO = 7 : 3.

the range of 50–700°C with the heating rate of 10°C/min under nitrogen flow. The samples were measured in a sealed aluminium pan with an initial mass of about 6 mg.

Mechanical testing was performed using a uniaxial testing machine (INSTRON1185) with crosshead speed of 10 mm/min and gauge length of 5 cm. The samples were prepared in strip shape with dimensions of 10 cm (length) × 1 cm (width). The thicknesses of the samples were measured using a DUALSCOPE MPO digital micrometer having a precision of 1 μm, and 10 different points for each specimen were measured to get an average thickness. At least five specimens were tested for each sample.

3. Results and Discussion

3.1. Structure and Morphology. According to some clay scientists, an assembly of layers can be referred to as a "particle" and an assembly of particles as an "aggregate" [14]. And these so-called MMT aggregates have three different spaces, that is, interlayer space, interparticle space, and interaggregate space [15]. These definitions also apply to GO, which has similar layered structures as MMT. And the interaction between MMT and GO can be well illustrated by tracking the changes of these three spaces before and after the self-assembly.

3.1.1. XRD Analysis of MMT/GO Hybrids. Figure 1 inset shows the digital photographs of MMT and GO hybrids. It can be seen that, for pure GO hybrids, their dispersions in DMF were not stable. After 24 h standing, GO nanolayers formed agglomerated structure and precipitated at the bottom of the bottle, while MMT, which was organically modified by CTAB, formed stable colloidal dispersions of solvated, anisotropic two-dimensional nanolayers in DMF. After blending the two dispersions by magnetic stirring and sonication, they could be reassembled to form interlayered composites. As expected, organically modified MMT nanoplatelets showed good capability in stabilizing GO in organic solvent.

In Figure 1, the XRD patterns of pristine MMT, GO, and their composites at different weight ratios are presented. For pristine MMT, a sharp characteristic diffraction peak exhibited at $2\theta \approx 6.919^\circ$ was clearly presented, which was assigned to the basal spacing of (001) reflection. After blending with GO, the characteristic peak still remained but only slightly shifted to lower angle (as seen in Table 1), and its shape became broader with decreased intensity, indicating that the effects between MMT and GO did not change the original layered structure of MMT. Besides, the peak left shift implied that the gallery height was slightly increased (as shown in Table 1), which was attributed to the DMF intercalation [16, 17].

The pattern of pristine GO showed the (001) reflection peak at $2\theta \approx 8.981^\circ$. For the complexes, only when the weight ratio of GO reached 30%, a small peak with relatively low intensity could be seen in the XRD pattern. The peak showed a slightly right shift, indicating a decreased d(001) spacing. As is known, no diffraction peak can be shown by the completely exfoliated GO, which means only the GO stacked together forming an ordered structure may contribute to the characteristic peak which appeared on the XRD pattern. The stacked GO nanoplatelets lost their interstratified water [18] during sonication in DMF which has been proved to have less affinity to GO than water [19], resulting in a decreased interlayer spacing.

3.1.2. Surface Morphology and Phase Uniformity. Figure 2 and Table 1 show the surface topography and the derived information of MMT and MMT/GO blends, respectively.

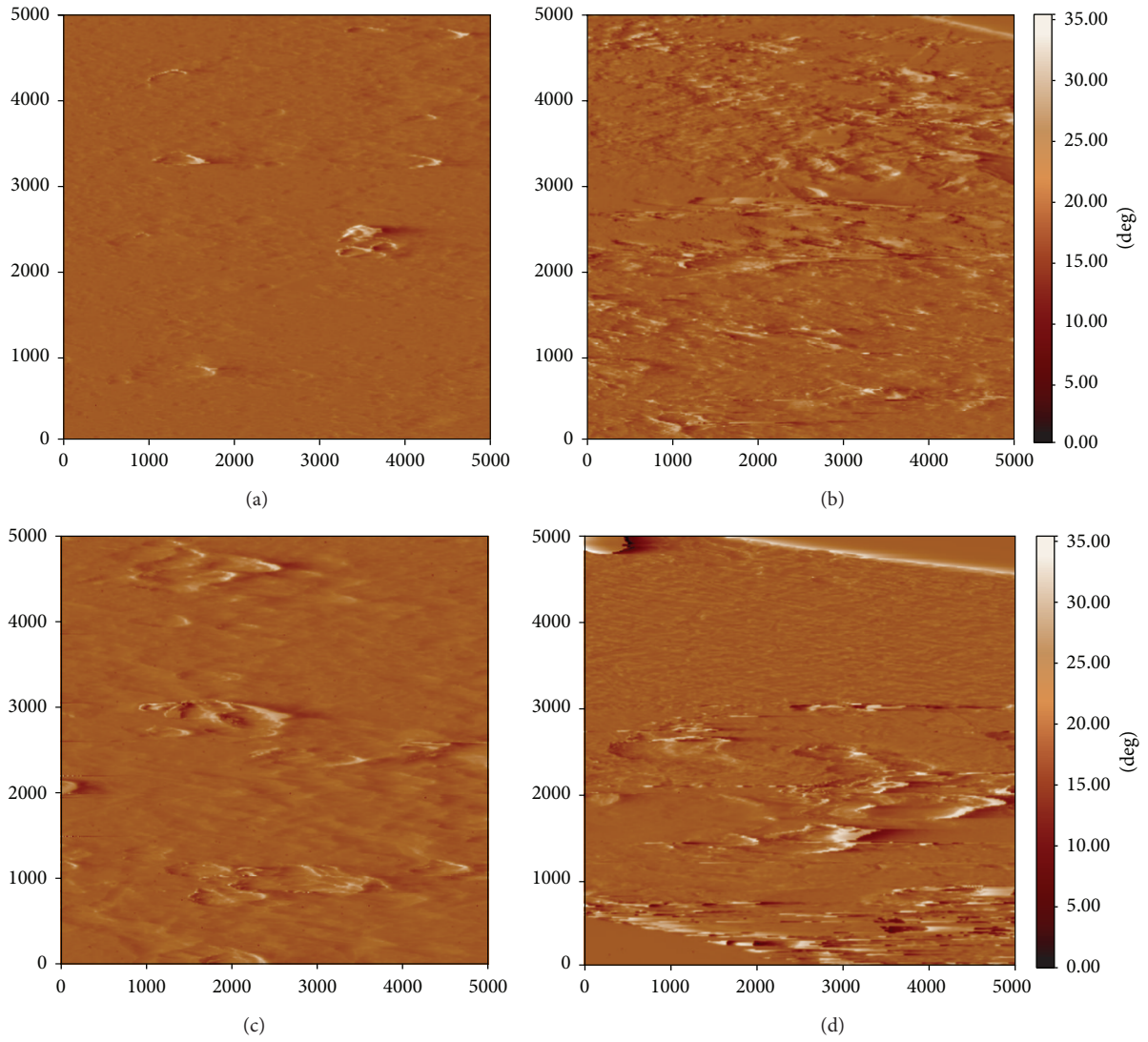

Figure 3: Phase contrast images of the MMT and MMT/GO complexes: (a) MMT, (b) MMT : GO = 9 : 1, (c) MMT : GO = 8 : 2, and (d) MMT : GO = 7 : 3.

Table 1: Physical properties of the nanoaggregates derived from XRD and AFM.

Composition	XRD		AFM topography image			
	2θ (°)	d-spacing (Å)	Average height (nm)	Average dimension of the first population length × width (nm)	Average dimension of the second population length × width (nm)	Surface roughness average (nm)
MMT	6.919	12.7655	116	507.81 × 156.25	71.09 × 30.88	10.1
MMT/GO 9 : 1	6.362	13.8816	242	585.94 × 176.05	146.81 × 56.94	25.6
MMT/GO 8 : 2	6.581	13.4204	242	762.72 × 157.47	206.01 × 48.83	26.7
MMT/GO 7 : 3	6.521	13.5423	238	722.72 × 156.25	323.59 × 107.42	31.5

As is shown in Figure 2, MMT and MMT/GO aggregates with different particle size and irregular shape were randomly distributed on top of the mica. It is known that the thickness of one single MMT sheet is approximately 1.2 nm [20], while the average height of those MMT aggregates shown in Figure 2(a) was as much as 116 nm (Table 1, calculated by Imager 4.60), indicating high agglomeration of MMT layers in DMF. With the addition of GO, the average height, the fractal dimension including two populations [20], and surface roughness of the hybrids were increased to more than

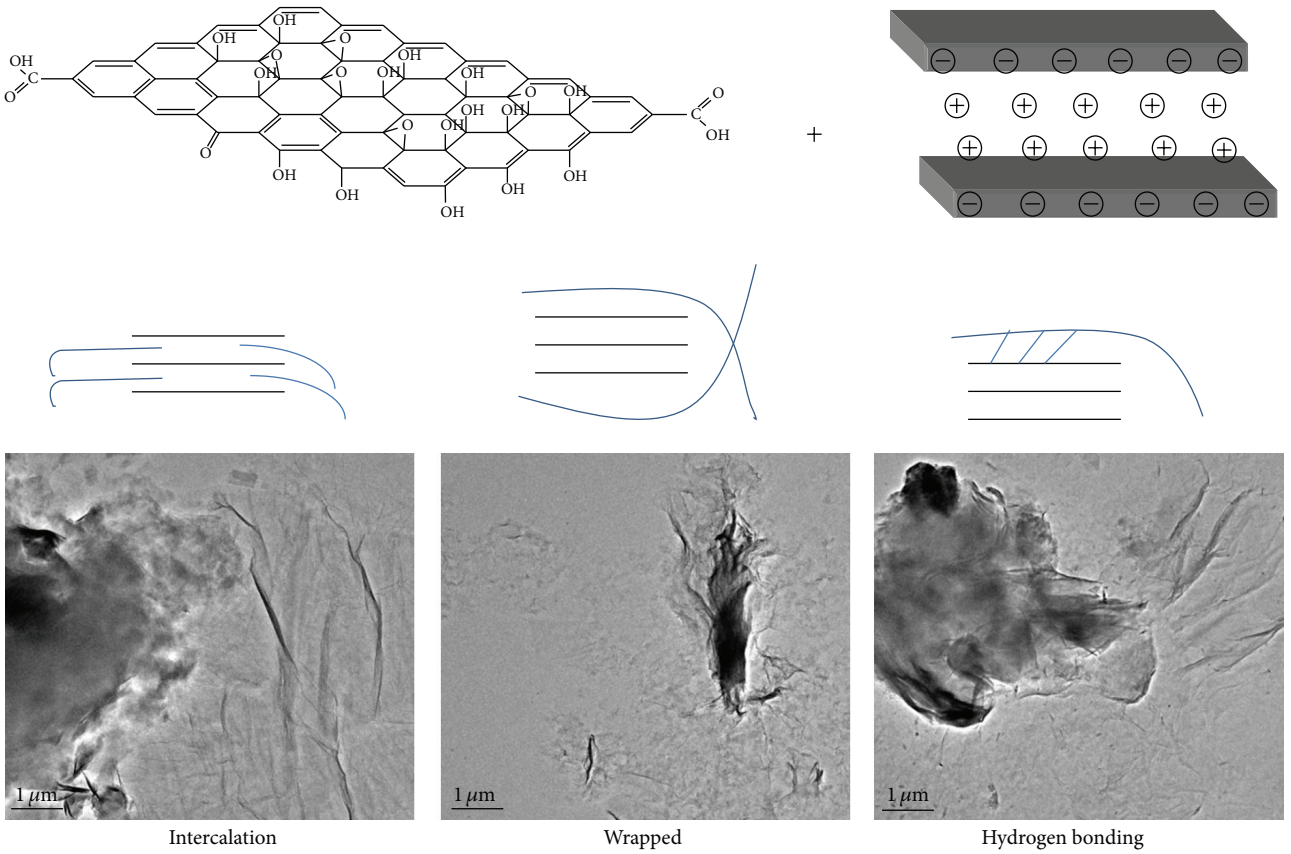

Figure 4: Proposed mechanism for the self-assembly effect of MMT and GO in DMF.

two times of the pristine MMT, whose result is consistent with the conclusion that the surface heterogeneity of a solid can contribute significantly to the fractal dimension [15]. The increase in surface roughness might lead to better adhesion with the polymer matrix.

According to some earlier published work [21, 22], the darker phase contrast indicated higher viscous/attractive force over the sample surfaces due to aggregated condensed matter, while the brighter phase contrast was seen when the tip penetrated a less viscous regime. The phase contrast images of MMT and MMT/GO complexes shown in Figure 3 are, respectively, corresponding to the topography images of the same sample illustrated in Figure 2. Significant effect on the phase morphology of MMT was observed upon addition of GO. The phase in the pure MMT was homogeneous, except a few bright areas caused by the sharp and high edges [23]. However, large phase shifts and phase variation were observed in the case of MMT/GO hybrids. The overall phase images became brighter than that of the pure MMT, indicating that a surface with higher rigidity was formed in this self-assembly process. This might be attributed to the more compact structure of MMT/GO hybrids, which will be further explained in the following section.

3.1.3. The Self-Assembly Behavior of MMT and GO in DMF. Herein, we propose a possible mechanism which is partially supported by TEM images to explain the effects between MMT and GO in the mutual-assisted dispersion, as shown in Figure 4. Intercalation, wrapping, and hydrogen bonding are considered as the main factors leading to self-assembly of MMT and GO in DMF. Intercalation behavior has also been proved by Kong and his coworkers [24], and similar TEM image has been provided in their work. But it needs to be further explained that this intercalation took place only in the interparticle space and interaggregate space. Based on the XRD analysis, the MMT in MMT/GO hybrids still well maintained its ordered layer structure. And the gallery height (0.2–0.4 nm) was far smaller than the thickness of GO (about 1 nm) [25], so it is impossible for GO to be intercalated into the interlayer structure. Hydrogen bonding has been proposed and explained by Zhang and his coworkers [11]. According to their work, the carboxyl groups on the GO sheets and the hydroxyl groups on the MMT nanoplatelets may form effective hydrogen-bonding interactions. Besides, the wrapping effect was also confirmed here by the TEM observations. These three types of physical interactions between GO and MMT nanoplatelets led to the formation of more compact MMT/GO hybrids in DMF, thus achieving a stable dispersion of GO sheets in DMF.

3.2. The Properties of the Electrospinning Solutions and the Morphology of the Resultant Electrospun Composite Nanofibers. As is known, the properties of the electrospinning solution including viscosity, surface tension, and

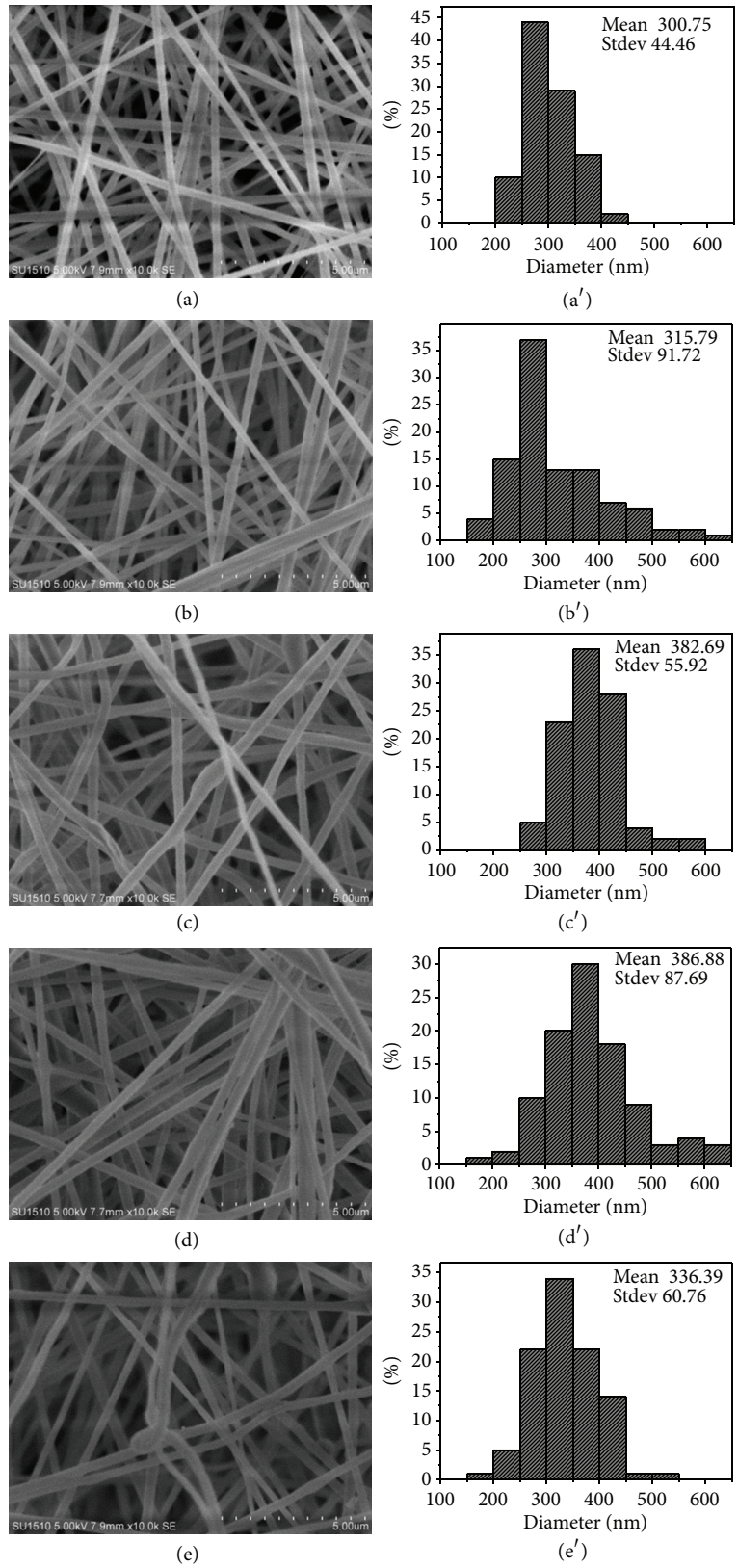

Figure 5: SEM images and diameter histogram distribution chart of PAN, PAN/MMT, and PAN/MMT-GO composite nanofibers: (a and a′) 0 wt. % MMT, (b and b′) 5 wt. % MMT, (c and c′) 5 wt. % MMT/GO, MMT : GO = 9 : 1, (d and d′) 5 wt. % MMT/GO, MMT : GO = 8 : 2, and (e and e′) 5 wt. % MMT/GO, MMT : GO = 7 : 3.

Table 2: The properties of electrospinning solution.

	Viscosity (mPa·s)	Conductivity (μS/cm)	Surface tension (mN/m)
PAN	162 ± 1.41	67.40 ± 0.10	27.277 ± 1.11
PAN/MMT	700.33 ± 1.70	61.50 ± 0.10	32.028 ± 0.26
PAN/MMT-GO-1	909.33 ± 1.53	65.10 ± 0.80	31.058 ± 0.11
PAN/MMT-GO-2	865 ± 3.26	70.40 ± 1.10	32.514 ± 1.22
PAN/MMT-GO-3	851.67 ± 1.15	76.45 ± 0.05	30.876 ± 0.80

conductivity affect the diameter of the resultant fibers. And it has been well proved that the decrease of surface tension and viscosity or the increase of solution conductivity favors the formation of thinner electrospun fibers [26]. As is presented in Table 2, upon the addition of nanofillers, the viscosity and surface tension were increased, while the conductivity decreased first and then increased, indicating a general trend of getting thicker fibers which is in correspondence with the mean diameter of the electrospun fibers shown in Figure 5 (a′–e′).

The structures of the electrospun pure PAN and PAN composite nanofibers with different nanofillers were investigated by SEM. As is shown in Figure 5, the morphology of the electrospun composite nanofibers was also slightly affected by the addition of nanofillers. Some beaded structures could be observed in the composite nanofibers, which can be attributed to some large aggregates incorporated inside the PAN nanofibers. This inference can be further confirmed by TEM observation.

The distribution of MMT/GO hybrid nanofillers in PAN nanofibers was investigated by HRTEM (Figure 6). Two populations of nanofillers exist in the PAN matrix, which is consistent with the observation from AFM topography images. Some MMT-rich nanofillers ("a" area) showed a stripe structure, which were well incorporated and oriented in the fiber axial direction. This was due to the higher draw ratio that imparted a larger stress on the fiber as it was being formed during the electrospinning process and gave rise to a proper alignment of the two-dimensional nanofillers along the fiber axis. However, some nanofillers ("b" area and "c" area) are just randomly distributed within the PAN matrix with cross-sectional orientation. This might be assigned to the GO-rich nanofiller, in which MMT was wrapped and cannot move freely to align along the fiber axis. Besides, with MMT/GO as nanofiller, the surface of the composite nanofibers became rough and irregular, which was in accordance with the results of SEM observations.

3.3. Thermal Properties of PAN Nanofibers with and without Nanofillers. The thermal stability of the pure PAN nanofibers and PAN composite nanofibers with different nanofillers is shown in Figure 7. Under pyrolytic conditions, PAN nanofibers with and without nanofillers degraded in two steps; more specifically, from 300 to 400°C was considered stage I while from 400 to 500°C was stage II. Compared with pure PAN nanofibers, the onset thermal decomposition temperature was respectively increased from ~300°C (pure PAN)

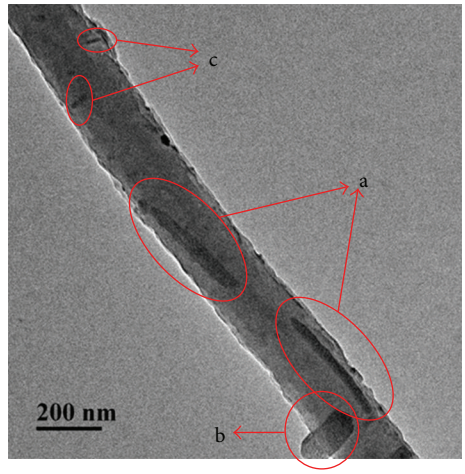

Figure 6: HRTEM images of PAN/MMT-GO-2.

to ~315°C (PAN/MMT) and ~330°C (PAN/MMT-GO-2), as is shown in Figures 7(a) and 7(b). This noticeable improvement in the decomposition temperature by MMT/GO composites could not be achieved by single MMT or GO nanoplatelet, according to the existing reports [27, 28]. The phenomenon might be ascribed to some synergistic effects of MMT and GO, whose layered structures may act as cross-bonding points and contribute to a stronger interaction between polymer chains and hybrid nanofillers, resulting in a highly enhanced thermal stability [28].

As is shown in Figure 7(c), a sharp weight loss was observed in stage I, which was due to the formation of the ring compounds among –CN groups. The nanofillers especially the hybrid ones had significant contribution to the decomposition of the composite nanofibers in this stage. While, in stage II during which further removal of nitrogen and building a better carbon backbone occurred, a relatively slower decomposition was observed. In general, the incorporation of MMT/GO composites changed the thermal behavior of the polymer host.

3.4. Mechanical Properties. The mechanical properties of the electrospun PAN nanofibers with and without nanofillers were investigated by the tensile stress-strain testing method and the results are given in Table 3. All the nanofillers enhanced the strength of PAN to various extents. With the addition of only MMT, the ultimate tensile strength increased by only 10.7%, while, for MMT/GO composite nanofillers with the weight ratio as 9 : 1, it increased by 32%, which was the highest among the hybrid nanofillers investigated here. With the further increase of GO ratio, the tensile strength was slightly decreased, probably due to the aggregation of the two different nanoplatelets and forming large particles that could not be uniformly distributed within the PAN matrix. As for the result of elongation at break, a general trend of decrease was observed, indicating a loss of elasticity after the incorporation of the nanofillers. This result is consistent with some published works [5, 6, 13]. Generally, compared

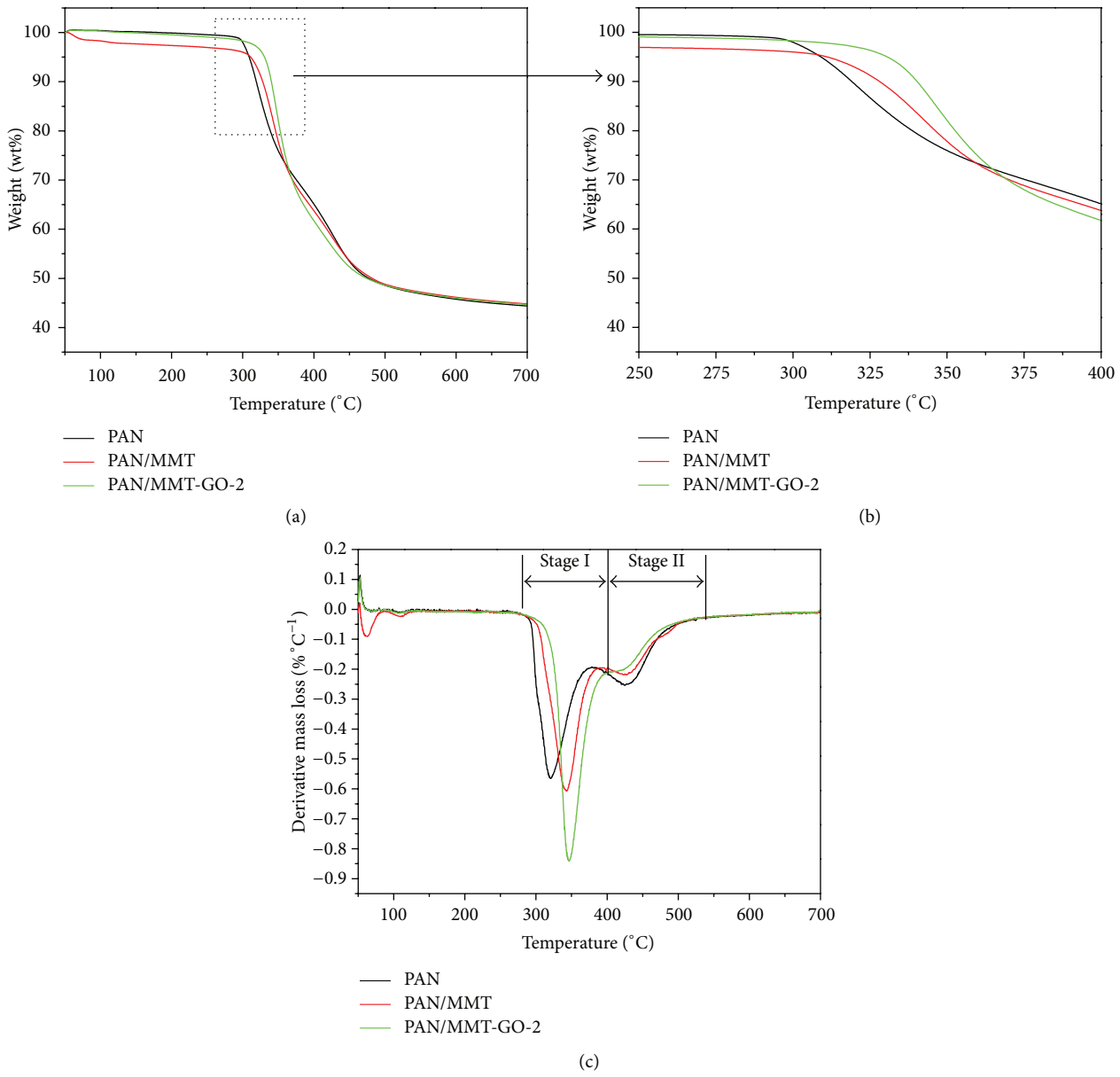

Figure 7: Thermogravimetric curves (a) and corresponding derivative curves (c) of PAN, PAN/MMT, and PAN/MMT-GO-2; (b) is a magnified image of selected area of (a).

with MMT, the hybrid MMT/GO nanofiller showed better performance in reinforcement.

4. Conclusion

In summary, MMT/GO composite nanofillers were successfully prepared and well stabilized in DMF solution by self-assembly behavior which can be further divided into three effects, that is, intercalation between the interparticle space and interaggregate space, wrapping, and hydrogen bond. The inference was examined by XRD, AFM, and TEM. Then, the composite nanofillers were well incorporated into the PAN matrix by electrospinning technique. Compared with MMT, the MMT/GO composite nanofillers showed better thermal and mechanical properties. Besides, the morphology of the electrospun PAN nanofibers with MMT/GO used as

Table 3: Mechanical properties of PAN with and without nanofillers.

	Tensile strength (MPa)	Elongation at break (%)
PAN	6.06 ± 0.82	75.26 ± 6.06
PAN/MMT	6.71 ± 1.28	26.61 ± 4.69
PAN/MMT-GO-1	8.00 ± 1.06	38.50 ± 5.14
PAN/MMT-GO-2	7.86 ± 0.57	39.10 ± 4.54
PAN/MMT-GO-3	7.55 ± 1.40	39.43 ± 6.00

nanofillers was also desirable. So, MMT/GO hybrid nanofiller is an attractive candidate for thermal stability improvement and mechanical reinforcement material.

Conflict of Interests

The authors declare that there is no conflict of interests regarding the publication of this paper.

Acknowledgments

The authors would like to acknowledge the financial support from the National High-tech R&D Program of China (no. 2012AA030313), Changjiang Scholars and Innovative Research Team in University (no. IRT1135), and the Priority Academic Program Development of Jiangsu Higher Education Institutions.

References

[1] C. Nethravathi, B. Viswanath, C. Shivakumara, N. Mahadevaiah, and M. Rajamathi, "The production of smectite clay/graphene composites through delamination and co-stacking," *Carbon*, vol. 46, no. 13, pp. 1773–1781, 2008.

[2] M. Yousfi, J. Soulestin, B. Vergnes, M. F. Lacrampe, and P. Krawczak, "Morphology and mechanical properties of PET/PE blends compatibilized by nanoclays: effect of thermal stability of nanofiller organic modifier," *Journal of Applied Polymer Science*, vol. 128, no. 5, pp. 2766–2778, 2013.

[3] G.-M. Kim, D.-H. Lee, B. Hoffmann, J. Kressler, and G. Stöppelmann, "Influence of nanofillers on the deformation process in layered silicate/polyamide-12 nanocomposites," *Polymer*, vol. 42, no. 3, pp. 1095–1100, 2001.

[4] M. Zhang and U. Sundararaj, "Thermal, rheological, and mechanical behaviors of LLDPE/PEMA/clay nanocomposites: effect of interaction between polymer, compatibilizer, and nanofiller," *Macromolecular Materials and Engineering*, vol. 291, no. 6, pp. 697–706, 2006.

[5] H. Mattausch, S. Laske, I. Duretek, J. Kreith, G. Maier, and C. Holzer, "Investigation of the influence of processing conditions on the thermal, rheological and mechanical behavior of polypropylene nanocomposites," *Polymer Engineering & Science*, vol. 53, no. 5, pp. 1001–1010, 2013.

[6] H. Q. Fu, C. Yan, W. Zhou, and H. Huang, "Preparation and characterization of a novel organic montmorillonite/fluorinated waterborne polyurethane nanocomposites: effect of OMMT and HFBMA," *Composites Science and Technology*, vol. 85, pp. 65–72, 2013.

[7] B. Z. Jang and A. Zhamu, "Processing of nanographene platelets (NGPs) and NGP nanocomposites: a review," *Journal of Materials Science*, vol. 43, no. 15, pp. 5092–5101, 2008.

[8] J. Liang, Y. Huang, L. Zhang et al., "Molecular-level dispersion of graphene into poly(vinyl alcohol) and effective reinforcement of their nanocomposites," *Advanced Functional Materials*, vol. 19, no. 14, pp. 2297–2302, 2009.

[9] M. A. Rafiee, J. Rafiee, Z. Wang, H. Song, Z.-Z. Yu, and N. Koratkar, "Enhanced mechanical properties of nanocomposites at low graphene content," *ACS Nano*, vol. 3, no. 12, pp. 3884–3890, 2009.

[10] X. Yang, Y. Tu, L. Li, S. Shang, and X.-M. Tao, "Well-dispersed chitosan/graphene oxide nanocomposites," *ACS Applied Materials and Interfaces*, vol. 2, no. 6, pp. 1707–1713, 2010.

[11] C. Zhang, W. W. Tjiu, W. Fan, Z. Yang, S. Huang, and T. Liu, "Aqueous stabilization of graphene sheets using exfoliated montmorillonite nanoplatelets for multifunctional free-standing hybrid films via vacuum-assisted self-assembly," *Journal of Materials Chemistry*, vol. 21, no. 44, pp. 18011–18017, 2011.

[12] P. Xu, J. Loomis, B. King, and B. Panchapakesan, "Synergy among binary (MWNT, SLG) nano-carbons in polymer nanocomposites: a Raman study," *Nanotechnology*, vol. 23, no. 31, Article ID 315706, 2012.

[13] P. A. Song, L. N. Liu, S. Y. Fu et al., "Striking multiple synergies created by combining reduced graphene oxides and carbon nanotubes for polymer nanocomposites," *Nanotechnology*, vol. 24, no. 12, Article ID 125704, 2013.

[14] J. Du, R. A. Pushkarova, and R. S. C. Smart, "A cryo-SEM study of aggregate and floc structure changes during clay settling and raking processes," *International Journal of Mineral Processing*, vol. 93, no. 1, pp. 66–72, 2009.

[15] J. Zhu, L. Zhu, R. Zhu, S. Tian, and J. Li, "Surface microtopography of surfactant modified montmorillonite," *Applied Clay Science*, vol. 45, no. 1-2, pp. 70–75, 2009.

[16] N. Salahuddin, S. A. Abo-El-Enein, A. Selim, and O. Salah El-Dien, "Synthesis and characterization of polyurethane/organo-montmorillonite nanocomposites," *Applied Clay Science*, vol. 47, no. 3-4, pp. 242–248, 2010.

[17] C. Breen, F. Clegg, T. L. Hughes, and J. Yarwood, "Distinguishing interlayer cations in montmorillonite by thermal analysis of dimethylformamide-saturated samples," *Journal of Physical Chemistry B*, vol. 105, no. 21, pp. 4872–4878, 2002.

[18] O. C. Compton, S. W. Cranford, K. W. Putz et al., "Tuning the mechanical properties of graphene oxide paper and its associated polymer nanocomposites by controlling cooperative intersheet hydrogen bonding," *ACS Nano*, vol. 6, no. 3, pp. 2008–2019, 2012.

[19] K. W. Putz, O. C. Compton, M. J. Palmeri, S. T. Nguyen, and L. C. Brinson, "High-nanofi ller-content graphene oxide-polymer nanocomposites via vacuum-assisted self-assembly," *Advanced Functional Materials*, vol. 20, no. 19, pp. 3322–3329, 2010.

[20] A. Cadene, S. Durand-Vidal, P. Turq, and J. Brendle, "Study of individual Na-montmorillonite particles size, morphology, and apparent charge," *Journal of Colloid and Interface Science*, vol. 285, no. 2, pp. 719–730, 2005.

[21] G. Haugstad, W. L. Gladfelter, and R. R. Jones, "Tip-sample interactions in dynamic force microscopy of polyvinyl alcohol films," *Polymer International*, vol. 49, no. 5, pp. 427–431, 2000.

[22] R. Dong and L. E. Yu, "Investigation of suflace changes of nanoparticles using TM-AFM phase imaging," *Environmental Science and Technology*, vol. 37, no. 12, pp. 2813–2819, 2003.

[23] W. W. Scott and B. Bhushan, "Use of phase imaging in atomic force microscopy for measurement of viscoelastic contrast in polymer nanocomposites and molecularly thick lubricant films," *Ultramicroscopy*, vol. 97, no. 1–4, pp. 151–169, 2003.

[24] Y. Kong, Y. Xu, H. Mao, C. Yao, and X. Ding, "Expanded graphite modified with intercalated montmorillonite for the electrochemical determination of catechol," *Journal of Electroanalytical Chemistry*, vol. 669, pp. 1–5, 2012.

[25] Y. Wang, Z. Shi, and J. Yin, "Facile synthesis of soluble graphene via a green reduction of graphene oxide in tea solution and its biocomposites," *ACS Applied Materials and Interfaces*, vol. 3, no. 4, pp. 1127–1133, 2011.

[26] C. Wang, H.-S. Chien, C.-H. Hsu, Y.-C. Wang, C.-T. Wang, and H.-A. Lu, "Electrospinning of polyacrylonitrile solutions at elevated temperatures," *Macromolecules*, vol. 40, no. 22, pp. 7973–7983, 2007.

[27] Q. Bao, H. Zhang, J.-X. Yang et al., "Graphene-polymer nanofiber membrane for ultrafast photonics," *Advanced Functional Materials*, vol. 20, no. 5, pp. 782–791, 2010.

[28] H. Qiao, Y. Cai, F. Chen et al., "Influences of organic-modified Fe-montmorillonite on structure, morphology and properties of polyacrylonitrile nanocomposite fibers," *Fibers and Polymers*, vol. 10, no. 6, pp. 750–755, 2009.